European Polymer Journal 67 (2015) 242–251

Contents lists available at ScienceDirect

European Polymer Journal

journal homepage: www.elsevier.com/locate/europolj

Macromolecular Nanotechnology

Chitosan/silver nanocomposites: Synergistic antibacterial action of silver nanoparticles and silver ions

Siva Kumar-Krishnan [a], Evgen Prokhorov [a], Monserrat Hernández-Iturriaga [b], Josué D. Mota-Morales [a], Milton Vázquez-Lepe [c], Yuri Kovalenko [a], Isaac C. Sanchez [d], Gabriel Luna-Bárcenas [a,*]

[a] Centro de Investigación y de Estudios Avanzados del IPN, Querétaro 76230, Qro., Mexico
[b] Universidad Autónoma de Querétaro, Querétaro 76010, Mexico
[c] Departamento de Ingeniería de Proyectos, Universidad de Guadalajara, 44430, Mexico
[d] Department of Chemical Engineering, The University of Texas at Austin, Austin, TX 78712, United States

ARTICLE INFO

Article history:
Received 20 January 2015
Received in revised form 25 March 2015
Accepted 29 March 2015
Available online 7 April 2015

Keywords:
Chitosan nanocomposite
Silver nanoparticles/ions
Antimicrobial activity
Electrical conductivity
Percolation threshold

ABSTRACT

In the present work chitosan–silver (CS/Ag) nanocomposites, either in the form of nanoparticles (AgNP) or as ionic dendritic structures (Ag^+), are synthesized by a simple and environmentally friendly *in situ* chemical reduction process. The antibacterial activity of the resulting nanocomposites in the form of films is studied against two bacteria, Gram-positive *Staphylococcus aureus* and Gram-negative *Escherichia coli*. The relationship between electrical, structural and antibacterial properties of CS/AgNP and CS/Ag^+ nanocomposites are studied by transmission electron microscopy (TEM), scanning electron microscopy (SEM), X-ray diffraction, and UV–Vis, impedance, infrared and X-ray photoelectron spectroscopies. The results demonstrate that in contrast to CS/Ag^+ ion films, the CS/AgNP composites films (average particle size less than 10 nm) showed a significantly higher antibacterial potency. The collective action of AgNP and Ag^+ ions facilitate the enhancement and synergetic antibacterial activity below certain critical concentration. The bactericide activity of both CS/AgNP and CS/Ag^+ ion composite films increases by increasing the concentration of Ag. The composites containing 1 wt.% of silver nanoparticles and about of 2 wt.% of silver ions exhibit a maximum antibacterial activity, which is close to their electrical percolation threshold. The concentration of AgNP and Ag^+ ions above the threshold level greatly diminish the antibacterial potential.

1. Introduction

In recent years the development of efficient and greener routes for metal nanoparticles syntheses has gained considerable interest in various areas of nanotechnology. Among metal nanoparticles, silver nanoparticles (AgNP) have attracted much attention due to their potential as antimicrobial agent; they are widely applied in many biological and medical fields such as biosensors, wound healing, treat burns and cancer therapeutics [1–4]. Several AgNP based composites have been demonstrated enhanced performance through the stabilization and support of nanoparticles [5,6]. Regarding silver-based nanocomposites, chitosan–silver nanoparticles (CS/AgNP) nanocomposites represents an emerging group of bio-nanostructured hybrid materials because of its biocompatibility and biodegradability. CS is considered a non-toxic biopolymer, aside of its excellent antimicrobial and antifungal activities against a wide range of

* Corresponding author. Tel.: +52 (442)211 9900.
E-mail address: gluna@qro.cinvestav.mx (G. Luna-Bárcenas).

http://dx.doi.org/10.1016/j.eurpolymj.2015.03.066
0014-3057/

microorganisms when compared to other polymers and biopolymers [7,8].

Several physical and chemical approaches have been established to prepare CS/AgNP composite films. Recent studies reported about direct dispersion of AgNPs into chitosan matrix for antibacterial applications [9]. However, common methods involve the chemical reduction of silver salts by different reducing agents such as $NaBH_4$, sodium citrate, or ascorbic acid [10–12]. However, in such chemical processes the nanoparticles tend to aggregate due to the high surface energy inherent to the synthesis. The reducing agents used for the preparation might exhibit environmental toxicity. Residuals of the chemical reduction processes could also affect the interaction with OH and NH_3^+ (or NH_2) functional groups of chitosan biopolymer. Therefore the composite's physicochemical and electrical properties can be greatly affected, and in consequence its antibacterial properties may eventually be affected as well. It was found that AgNP prepared from sodium borohydride reduction process causes cytoprotective effect on human immuno-deficiency virus infected cells [13]. Hence, a greener and environmental friendly approach for the synthesis and stabilization of nanoparticles using biopolymers present clear benefits. Biopolymers such as chitosan offer control over the rate of the chemical reduction process, thus enabling the synthesis and stabilization of nanoparticles with different size and shapes without the use of additional capping agents [14]. The stability of silver nanoparticles against agglomeration is considered the most important factor for their antibacterial efficacy in nanocomposites; the interaction of bacteria with AgNPs is more intensive when AgNPs are well dispersed [15]. It was reported in previous studies with phosphotriazine/diamine polymers that such type of stabilization together with an *in situ* greener synthesis route of polymer/silver nanocomposites exhibited higher antibacterial efficacy against many bacterial species [16]. On the other hand, some reports show that fabrication of asymmetric or porous chitosan film impregnated with AgNPs enhances the controlled release antibacterial activity [17–19].

Silver is commonly used in both ionic form and silver nanoparticles as antibacterial agents. Several studies have previously reported on the antibacterial activity of silver nanoparticles and the effect of size, concentration, temperature or ionic strength over its antibacterial properties [20–22]. Those properties are extensive to polymer–silver nanocomposites. For instance, Triebel et al. [23] reported polyurethane/silver nanocomposites with enhanced silver ion release using multifunctional invertible polyester. Tamboli et al. [24] evaluated the antibacterial activity of Ag–PANI nanocomposites against *B. subtilis*. The releasing of silver ions plays a crucial role in the antibacterial activity of AgNP by generating reactive oxygen species (ROS) upon exposure to the cells [25]. In addition, silver ions alone have profound antibacterial action towards Gram-positive *Staphylococcus aureus* and Gram-negative *Escherichia coli* [26]. Recently reported by Greulich et al. [27], there is evidence that the antibacterial activity of AgNP and Ag^+ ions (such as silver acetate) occurs in the bacteria and human cells in the same concentration range. Sotiriou and Pratsinis [28] showed the antibacterial activity of silver ions and silver nanoparticles immobilized into SiO_2 support. Additionally, several studies propose that metallic AgNP may attach to the surface of the cell membrane disturbing permeability and respiration functions of the cell [29,15]. Another scenario is that metallic AgNP not only interact with the surface of membrane but they can also penetrate the bacteria [30]. However, the mechanism of antibacterial action of AgNP and Ag^+ ions are poorly understood and there is a few knowledge on the toxicity of metallic AgNP by direct comparison with Ag^+ ions due to difficulties in controlling size, shape and agglomeration effects.

In this work we report a simple and efficient greener route to synthesize CS/metallic AgNP and CS/Ag^+ ions (silver acetate form) composite films using dilute acetic acid as a reducing agent, mediated by the biopolymer chitosan. The antibacterial activity of both silver metallic nanoparticle and silver ion containing chitosan films with different concentration were tested on Gram-positive and Gram-negative bacterias, *S. aureus* and *E. coli* respectively. Our method allows the *in situ* synthesis and stabilization of CS/AgNP and Ag^+ ions in a chitosan matrix while providing a direct comparison of antibacterial activity of silver metallic nanoparticles and silver ions in the same concentration range. To the best of our knowledge, this is the first report where the bactericidal effect of silver ions dendritic structures and silver nanoparticles reduced by dilute acetic acid and chitosan-mediated is evaluated through direct comparison. Also, a correlation between AgNP and Ag ions concentration in the nanocomposites with electrical properties and its antibacterial activity is proposed.

2. Materials and methods

2.1. Materials

Chitosan medium molecular weight (M_w = 300 kDa and 82% of degree of deacetylation) was purchased from Sigma–Aldrich (St. Louis, MO). Silver nitrate ($AgNO_3$) and acetic acid (glacial, 99–100%: Merck) were also purchased from Sigma Aldrich. Chitosan solution was obtained by dissolving 1 wt.% of CS powder in 1% aqueous acetic acid solution and was subsequently stirred to promote dissolution. All reagents are analytical grade and used without further purification. All glass containers were washed and rinsed with deionized water.

2.1.1. Preparation of CS/AgNP composite film

The synthesis was carried out by adding 100 μl of different concentrations of silver precursor $AgNO_3$ (0.01, 0.05, 0.1, 0.2, 0.3, 0.4, 0.5, 0.6 and 0.8 M) to 10 ml of chitosan solution in acetic acid (1%) and the final solution was magnetically stirred at 95 °C, then allowed to react for an additional 8 h. The color of the solution progressed from colorless to light yellow within 30 min, and finally to dark yellow after the reaction completed. This change of color indicates the formation of AgNP. The temperature of the reaction plays an important role as it has a strong influence on the particle size and dispersion of AgNP in the chitosan solution. CS/AgNP films were obtained by

the solvent cast method pouring the final solution into a plastic Petri dish and allowing the solvent to evaporate for 24 h at 60 °C. Confirmation that in this case most of AgNP were in metallic state will be described below based on XRD and XPS measurements.

2.1.2. Preparation of CS/Ag^+ ion composite film

The CS/Ag^+ ion colloidal solution was obtained by adding 100 μl of different concentrations of prepared $AgNO_3$ (0.01, 0.05, 0.1, 0.2, 0.3, 0.4, 0.5, 0.6 and 0.8 M) to 10 ml of chitosan solution in acetic acid (1%), and the final solution was allowed to magnetically stirred for 4 h at room temperature (25 °C). Composite films were obtained by the solvent cast method by pouring the final solution into a plastic Petri dish and allowing the solvent to evaporate for 24 h at 60 °C. It is noteworthy that both CS/AgNP films and CS/Ag^+ ion composite films are non-neutralized. Confirmation that in this case the CS/Ag^+ ion composite films (CS/silver acetate as a source of silver ions [27]) have been obtained will be described below based on UV–Vis, XRD and XPS measurements.

2.2. Methods

The formation of AgNP was monitored by UV–Vis spectroscopy (UV–Vis spectrophotometer: Agilent 8453). The morphology of CS/AgNP films was analyzed by JEOL JEM-1010 transmission electron microscope (TEM) operated at 80 kV. CS/Ag^+ ion films were analyzed by JEOM JSM-7401F field emission scanning electron microscope (SEM). The weight percent of silver in CS nanocomposite films have been analyzed by energy dispersive analysis (EDS). Analysis of the composites structure was performed by Fourier transform infrared spectroscopy (FTIR) on a Perkin Elmer spectrophotometer using an ATR accessory in the range 4000–650 cm^{-1}. Films were dried at 60 °C for 24 h before performing the FT-IR measurements to decrease the influence of moisture content. Impedance measurements, in the frequency range of 100 Hz to 110 MHz, were carried out using an Agilent Precision Impedance Analyzer 4294A. X-ray diffraction was performed using a Rigaku diffractometer ULTIMA IV, equipped with the Cu Kα radiation (λ = 1.5406 Å). X-ray photoelectron spectroscopy (XPS) was carried out using the Alpha110 instrument from ThermoFisher Scientific with a monochromatic Al kα_1 (1486.7 eV) X-ray source, and a hemispherical electron analyzer with seven channeltrons. The calibration of the binding energy of the spectra was performed with the C1s peak of the carbon due to C—C bonding at 284.8 eV. The peaks were fitting with the software AAnalyzer® v 1.1.

2.3. Bactericidal activity of CS/AgNP and CS/Ag^+ composite films

Strains of Gram-positive *S. aureus* (ATCC 8923) and Gram-negative *E. coli* (ATCC 25922) were tested. Squares of each film (1 × 1 cm) were aseptically obtained with a sanitized scalpel. Each square was inoculated with 10 μl (8 log CFU/square) and placed inside sterile glass tubes, and incubated at 22 °C for up to 24 h with the time interval of 0, 24 and 48 h. Films were removed from storage and placed in tubes containing 3 ml of Dey-Engley (DE) neutralizing broth (pH 7.6; BBL/Difco) and were homogenized using vortex for 1 min.

Inocula and inoculated CS/AgNP films and CS/Ag^+ ions films were analyzed for populations of bacteria. Cell suspensions were serially diluted in sterile 0.1% peptone and surface plated (0.1 ml) on tryptic soy agar supplemented with rifampicin (TSAR, 100 mg/ml). Inoculated plates were incubated at 35 °C for 24 h before colonies were counted. Colonies from each sample were chosen randomly and subjected to biochemical confirmation.

3. Results and discussion

3.1. UV–Vis spectroscopy analysis

The formation of AgNP obtained by reduction of different concentrations of $AgNO_3$ in the chitosan–dilute acetic acid solution at 95 °C was monitored by UV–Vis spectroscopy. Typical UV–Vis absorption spectra of the resulting solution are shown in Fig. 1. Specifically, in the case of sample prepared at 95 °C, the final solution starts to change from colorless to light yellow color within 20 min of reaction and further change to stable dark yellow color in 8 h after addition of $AgNO_3$ solution. It can be observed that all spectra display the characteristic surface plasmon resonance (SPR) absorption maximum between 412 nm and 416 nm, indicating the formation of spherical silver nanoparticles [31]. At the same time, it is evident from Fig. 1 that, as the concentration of precursor ($AgNO_3$) increases, a progressive increment in the intensity of the SPR band is observed which is related with an increase of AgNP concentration in the chitosan solution. It was found that the concentration of acetic acid in CS and temperature play an important role in the reduction process. These results are consistent with the previous studies of gold nanoparticles synthesis by dilute acetic acid used as reducing agent and chitosan as mediator of the reaction [32]. In contrast, the films prepared at room temperature exhibited a transparent aspect because silver nanoparticle formation

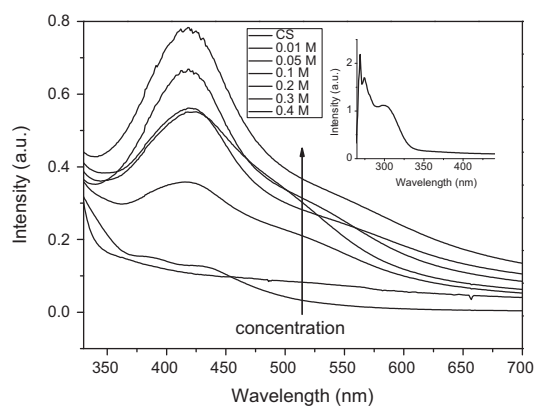

Fig. 1. UV–Vis absorption spectrum of CS/AgNP films obtained by reduction under different concentration of precursor ($AgNO_3$) at 95 °C. Inset shows UV–Vis absorption spectrum of CS/Ag + films obtained at 25 °C.

is not promoted by temperature. Accordingly, UV–Vis absorption spectra of such films did not show absorption peaks with maximum between 412 nm and 416 nm indicative of formation of metallic silver nanoparticles (inset in Fig. 1). Absorptions peaks centered between 270 and 300 nm are in place of those related to nanoparticles and can be assigned to different clusters of silver ions such as Ag^{+}, Ag^{2+}, Ag^{3+} [33–35]. This means that the majority of Ag^{+} ions chemically interact with the dilute acetic acid and form CS/silver acetate as a source of silver ions [27].

3.2. Morphology analysis (TEM and SEM)

Transmission electron microscope (TEM) images of CS/AgNP composite films are shown in Fig. 2. TEM results revealed that in films with low concentration of silver (0.5 wt.%) the formation of spherical silver nanoparticles with size ranging from 3 to 11 nm are distributed homogeneously in the CS matrix (Fig. 2a). However, for 1 wt.% (Fig. 1b and c) AgNP agglomerates was observed. SEM micrographs of the films obtained from CS/Ag^{+} ion films with the same concentration range as CS/AgNP composite are shown in Fig. 3. Interestingly CS/Ag^{+} ions films showed a dendritic structure and dendritic flowerlike structure in the chitosan films at higher concentrations e.g. 1, 3 and 4 wt.% (Fig. 3a–c).

According to UV–Vis spectroscopy analysis, these dendritic structures consist of chitosan–Ag^{+} ions structures. It is well known from literature that chitosan is able to sorb silver ions through different mechanisms (e.g. ion exchange and chelation) [36,37]. The interaction of silver ions with chitosan takes place through the amino and hydroxyl groups (see Section 3.3). That is why in the initial stages of reduction, small clusters of silver ions (Ag^{+}) are formed as well as silver metal particles. These clusters present typical absorption between 270 and 300 nm, while the metallic particles absorb at 412 nm [38,39]. In the next step of reduction these clusters grow and assembly into dendritic structures due to electrostatic attraction between —COO and —NH_3 groups of chitosan with the Ag^{+} ions [35]. Those structures have been previously observed using atomic force microscope [40].

As mentioned above, the nanocomposite films were prepared from precursor solutions with different $AgNO_3$ concentration. In order to compare the electrical and antibacterial properties of both types of films, i.e. CS/AgNP and CS/Ag^{+}, nanocomposites were obtained by two different methods to assure the same wt.% of silver. By using EDS analysis, the concentration of silver in the CS films was then calculated (Fig. 4).

3.3. FTIR analysis

To understand the molecular interactions of AgNP and Ag^{+} ions with chitosan, Fourier-transform infrared spectroscopy (FTIR) analysis was performed. Fig. 5a shows

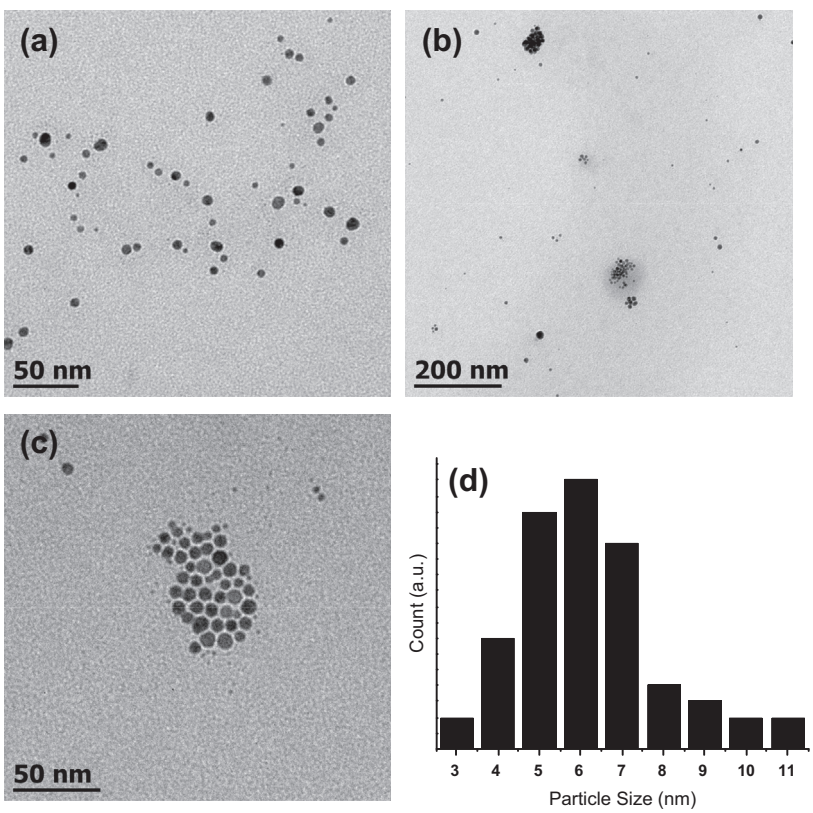

Fig. 2. TEM microphotograph of synthesized CS/AgNP composites: (a) 0.5 wt.% AgNP, (b) 1 wt.% AgNP, (c) higher magnification of 1 wt.% AgNP, and (d) size distribution of AgNP. The TEM micrographs were taken from colloidal suspension of AgNP in CS.

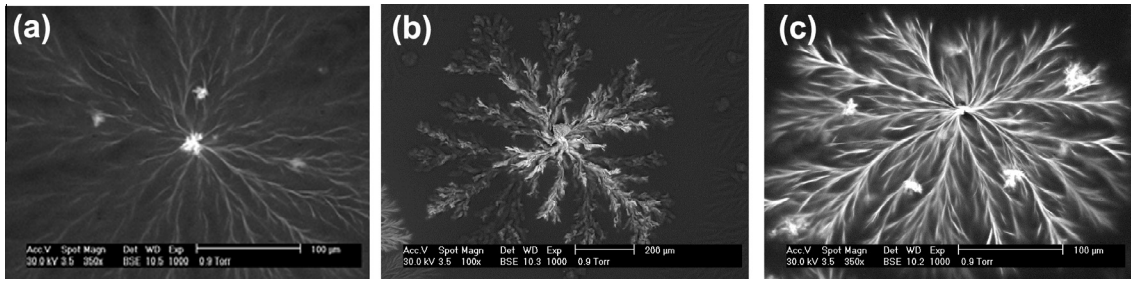

Fig. 3. SEM microphotograph of CS/Ag^+ ion composites: (a) 1 wt.%, (b) 3 wt.% and (c) 4 wt.% of Ag^+ ions in chitosan film (silver acetate form).

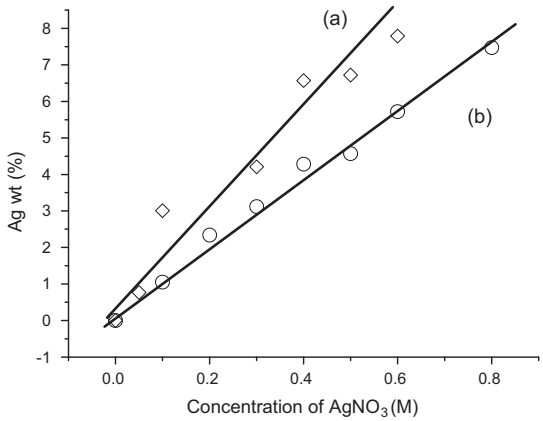

Fig. 4. Silver content by EDS analysis of (a) CS/AgNP composite and (b) CS/Ag + ion composite.

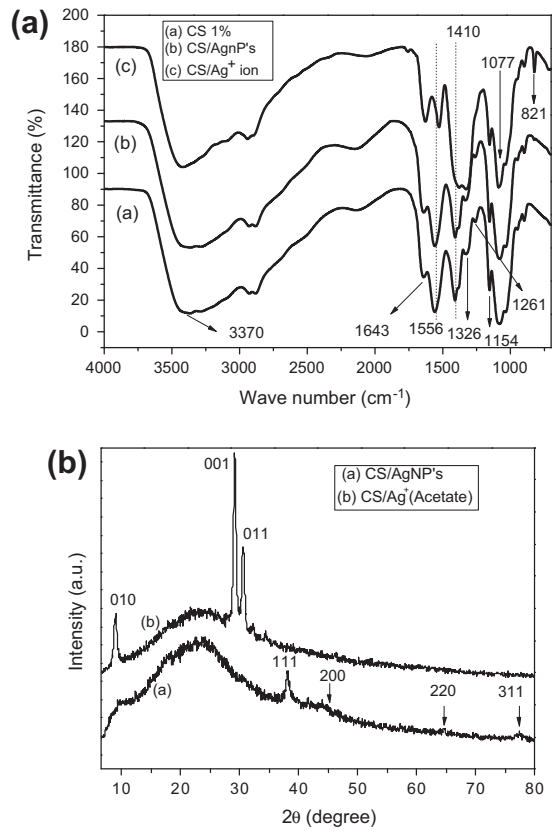

Fig. 5. (a) FTIR spectra of pristine CS, CS/AgNP and CS/Ag^+ ion composites. (b) X-ray diffraction pattern of CS/AgNP composites and (b) CS/Ag^+ ion (silver acetate) composites.

FTIR spectra of pristine CS, CS/AgNP and CS/Ag^+ ion composites films. The pure chitosan films exhibits characteristic transmittance band at 3000–3500 cm^{-1} assigned to the overlapped N—H and OH stretching vibrations [41] as well as vibration band at 1643 cm^{-1} band for amide I (C=O stretching), 1556 cm^{-1} for amide II (N—H bending), bands at 1410 cm^{-1} for OH bending vibrations, 1326 cm^{-1} for CH_2 wagging vibration, 1261 cm^{-1} for amide III vibration mode due to combination of N—H deformation and C—N stretching, and 1154 cm^{-1} for anti-symmetrical stretching of C—O—C bridge [42,43].

In the FTIR spectra of CS/AgNP nanocomposite film, the bands at 3370 cm^{-1} (amine and hydroxyl groups) and 1556 cm^{-1} (bending vibrations of NH_3) decrease in intensity and slightly shift to lower wave number evidencing the interaction of primary amino groups in chitosan with AgNP surface [42,44]. Other transmittance bands at 1643 cm^{-1} (amide I group), 1410 cm^{-1} (bending vibration of —OH group) and 1326 cm^{-1} (CH_2 wagging vibration) were not changed, suggesting that these transmittance bands are not sensitive to the metal nanoparticle surface [42].

In contrast to the CS/AgNP composite, the CS/Ag^+ ions films showed a significant decrease in transmittance in the band at 3370 cm^{-1}, it also shifts to 3430 cm^{-1}. The prominent N—H bending vibration bands around 1556 cm^{-1} shifted to 1539 cm^{-1} along with a decreasing in intensity, suggesting that the N—H vibration is strongly affected by the interaction with Ag^+ ions. On the other hand, the band at 1410 cm^{-1} (that corresponds to OH bending vibration), the bands near 1077 cm^{-1} (that are usually attributed to the C—O and C—N stretching vibrations) and the bands at 1326 cm^{-1} corresponded to CH_2 wagging vibrations, all showed a remarkable intensity reduction [42]. These changes are due to the interaction of hydroxyl groups with Ag^+ ions through oxygen [41]. Similar results have been reported in CS/Ag^+ ion films [45]. CS/Ag^+ ion composite film shows a new band about 821 cm^{-1} assigned to NO_3^- absorption, which confirms the existence of NO_3^- as a residual ion from silver salt.

Such band is not observed in CS/AgNP films, likely due to thermal decomposition of NO_3 to NO and O_2 [46].

Fig. 5b shows the X-ray diffraction patterns of CS/AgNP and CS/Ag^+ ion composite films. Typical XRD pattern of CS/AgNP composite film (5 wt.% of AgNP's) shows peaks at 2θ values of 38°, 44.2°, 64.3° and 77.7° that correspond to the (111), (200), (220) and (311) planes of face centered cubic (fcc) for Ag^0 [47]. The broad peak at 2θ equal 22.5° related to crystalline form of chitosan [48]. The crystalline size of nanoparticles d was estimated from XRD measurements using the Scherer formula. The calculated value of d was about of 9 ± 0.5 nm, which is close to TEM measurements.

In CS/Ag^+ ion composites, the characteristic peaks at 2θ values of 8.94°, 29.2° and 30.6° corresponded to the (010), (001) and (011) planes of silver acetate respectively. Typical peaks of AgNP at 2θ values of 38°, 44.2°, 64.3° and 77.7°, were not identified suggesting that silver was essentially in the form of silver acetate. The crystalline size of silver acetate was estimated from XRD measurements and equal to 14.6 ± 0.6 nm.

3.4. XPS analysis

X-ray photoelectron spectroscopy (XPS) analysis was performed by focusing on the changes of silver spectra to gain further insight into the specific interaction of AgNP and Ag^+ ions with chitosan. Two peaks (a doublet) characterize the Ag3d region of the silver; this is a consequence of spin orbital splitting that corresponds to $Ag3d_{3/2}$ and $Ag3d_{5/2}$ core levels. These two peaks are observed in the Ag3d region in CS/AgNP composite (Fig. 6a). The doublet can be further resolved into two components. In Fig. 6a, the peaks at 368.5 and 374.5 eV correspond to $3d_{5/2}$ and $3d_{3/2}$ core levels of metallic silver respectively [49], the spin–orbit components are separated by 6 eV, and the other component at lower binding energy (367.6 and 373.6 eV) indicate the presence of silver ions in Ag_2O with binding energy between 367.3 and 367.6 [50,51]. These results mean that 89.5% of silver is in metallic state. Conversely, in CS/Ag^+ ions composites (Fig. 6b) the deconvolution of Ag3d peak at 369.7 and 375.7 eV correspond to $3d_{5/2}$ and $3d_{3/2}$ core levels of Ag^+ ions, indicating that unreduced Ag^+ ions remain in the nanoparticles surface [52]. The peaks at lower binding energy (368.3 and 374.3) indicate the presence of metallic AgNP [49]. It is clear that 15% of original silver cations have been reduced to Ag^0 and the remaining 82.5% of silver exists in the ionic state. As a general conclusion from the XPS analysis, in CS/AgNP composite the majority of silver exists in Ag^0 state (lower oxidation states) and in the CS/Ag^+ ions composite films case, it exists as Ag^+ [53], in agreement with the UV–Vis observations. The additional 2.5% of peak observed at 366.7 eV can be related to higher oxidation state of silver as Ag_3O_4 [54].

A peak with binding energy at 406.5 eV (not shown) in the N 1s core-level has been observed in CS/Ag^+ ions composites, but not in CS/AgNP films. This peak can be attributed to NO_3^- ions [53]. These results relate well with FTIR measurements and confirm the thermal decomposition of NO_3^- ions at high temperature.

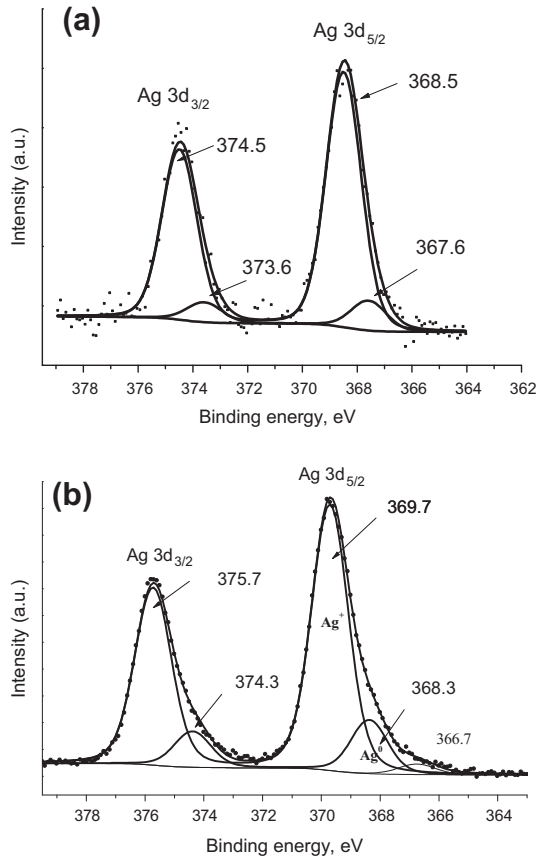

Fig. 6. XPS spectra for Ag3d region obtained on (a) CS/AgNP composites and (b) CS/Ag^+ ion composites.

3.5. Conductivity measurements

The DC conductivity of the composites was obtained from the extrapolation of impedance measurements to zero frequency and by using the dimensions of each film [55]. Neat chitosan exhibits low ionic conductivity that can be related to the presence of small concentration of conductive species in the form of OH^+ and H^+ ions [55]. At ambient conditions, film's water content is ca. 10 wt.%, which reduces the resistance of films and masks the real conductivity behavior of composites. Fig. 7a shows the plots of the DC electrical conductivity obtained from impedance measurements as a function of the AgNP and Ag ions wt.% in dry films at room temperature [55]. At low concentration of AgNP and Ag^+ ions, a decreasing in conductivity was observed. The decrease of conductivity in low concentration is explained by the strong interactions of AgNP and Ag^+ ions with free NH_3^+ groups of CS film, which in turns decrease the free H^+ and OH and are responsible for the conduction in CS [56]. An abrupt increasing of conductivity with increasing of both AgNP and Ag^+ ions wt.% and a subsequent saturation is typically observed for percolation phenomena.

CS/Ag^+ ion (silver acetate) composite films exhibited higher conductivity (approximately one order of magnitude) compared with CS/AgnP's composite films with the

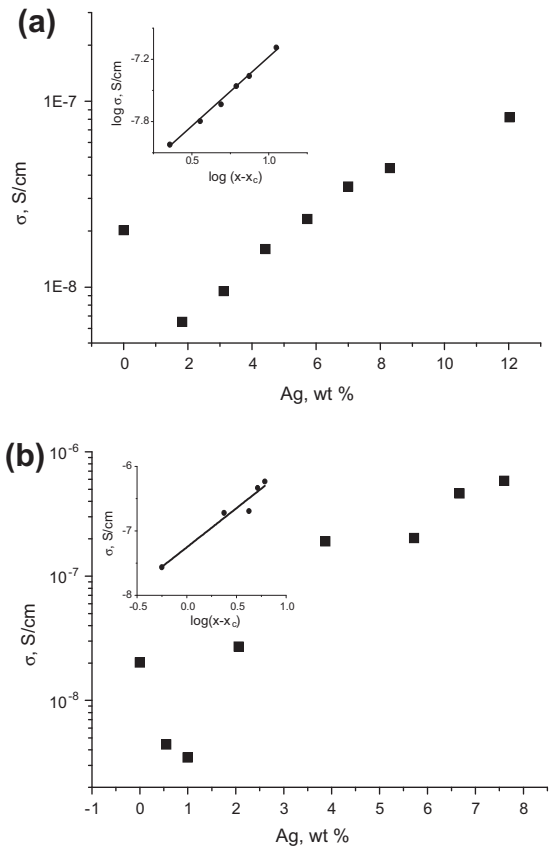

Fig. 7. Electrical conductivity of (a) CS/AgNP films as a function of the AgNP wt.% and (b) CS/Ag^+ films as a function of the Ag^+ wt.%. Inset shows a double log–log plot of the electrical conductivity versus $x - x_c$.

same Ag content (Fig. 7b). This enhanced conductivity is due to an increase in the concentration of Ag^+ ions, as expected. The XPS (X-ray photoelectron spectroscopy) analysis of CS/Ag^+ ions composites indicates the presence of 82.5% of silver in Ag^+ form.

It is important to note that CS–silver nanocomposites demonstrated low conductivity even in the saturation region. Such effect has been observed in films obtained by direct dissolved of silver nanoparticles in chitosan solution and has been explained by the presence of a thin polymer layer that coexists between silver nanoparticles [57].

In the vicinity of the percolation threshold a simple power law describes the DC conductivity as follow [58]:

$$\sigma \propto (x - x_c)^t, \quad \text{for } x > x_c \tag{1}$$

where x is the wt.% of conductivity phase, x_c is the critical AgNP concentration at the percolation threshold, and t is a critical exponent that only depends on the dimensionality of the percolation system. The insets in Fig. 7 show the log–log dependence of the conductivity of the CS composites on $x - x_c$. The least-square fitting analysis according to Eq. (1) results in a percolation threshold of 0.85 ± 0.31 wt.% of silver nanoparticles and a critical exponent t equals to 1.24 ± 0.11 for CS/AgNP films; whereas for CS/Ag^+ ions films the percolation threshold is 1.51 ± 0.21 wt.% and the critical exponent 1.21 ± 0.16. Values of critical exponent between 1 and 1.33 imply that the CS/silver nanoparticles system is two-dimensional according to well-established values [60]. The same value of critical exponent (1.32 ± 0.09) has been calculated in films obtained by direct dissolved silver nanoparticles in chitosan solution [57]. Such low value of the critical exponent clearly suggests that a 2D conductive network is formed and that charge must flow along surfaces and interstitial spaces of polymer matrix [60].

3.6. Antibacterial analysis

The antibacterial activity of as-synthesized CS/AgNP and CS/Ag^+ ions nanocomposites films was evaluated against Gram-positive bacteria *S. aureus*, and Gram-negative bacteria *E. coli*. We mainly focused on the concentration-dependent antibacterial activity of CS/AgNP and CS/Ag^+ ions nanocomposites, which provides direct toxicity comparison between AgNP and Ag^+ ions. In order to ensure the accuracy of the measurement, all films were subjected to antibacterial test simultaneously and under the same conditions. Additionally, our previous study demonstrated that dilute acetic acid present in the CS significantly influences the bacterial growth, so neutralization of films was carried out by washing them with deionized water until neutral pH (pH = 7).

The antibacterial activity of neat chitosan was reported previously [61]. However, the exact mechanism of antibacterial action of neat chitosan is not fully understood while several hypotheses have been proposed. Interaction of the protonated amino groups of chitosan with the negatively charged cell membranes surface [62], penetration into the phospholipid bilayer of membranes, and disruption of the cytoplasmic membrane are common explanations of the action of neat chitosan [63]. For instance, it has been observed a remarkably decreasing about two orders of magnitude of CFU/cm^2 of *S. aureus* after 48 h of cell culture in pristine chitosan films [64].

The antibacterial effect of both CS/AgNP and CS/Ag^+ ion composite films against *S. aureus* and *E. coli* incubated after 48 h are shown in Fig. 8. It can be seen that there is a slight difference in antibacterial effectiveness of both films against investigated Gram-positive *S. aureus*, suggesting that the relatively ten times thicker Gram positive cell wall with multiple murein layers and teichoic acid prevents the interaction of AgNP with thiol group, resulting in a decrement in bactericidal effect [65]. A similar observation has been reported in our previous studies of commercial AgNP embedded into chitosan matrix [64]. However, the CS/AgNP nanocomposites synthesized at 95 °C were found to be more efficient (approximately 2 orders of magnitude) than those CS/Ag^+ ion films prepared at room temperature (25 °C).

Additionally, Fig. 8 shows that the antibacterial effect for CS/AgNP films and CS/Ag^+ ions composite films clearly increased as increasing concentration of AgNP's and Ag^+ ions until it reaches a maximum at certain critical concentration that correlates well with the percolation threshold concentration determined by conductivity measurements (Fig. 7). CS/AgNP films with approximately 1 wt.% of silver

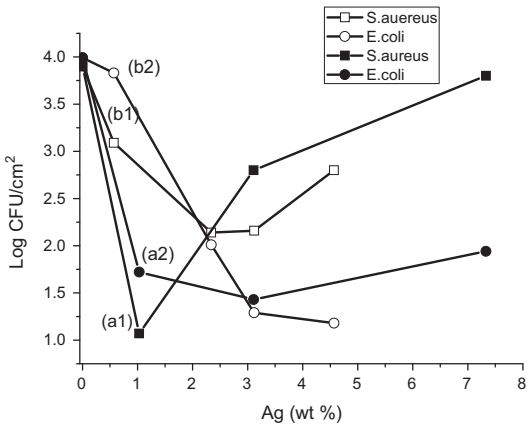

Fig. 8. Log CFU/cm^2 versus Ag concentration for CS/AgNP and CS/Ag$^+$ ion composites after 48 h of culture (a1, a2 for CS/AgNP composite films and b1, b2 for CS/Ag$^+$ ion composite films).

showed a minimum in CF/cm^2 (i.e. maximum bactericidal effect), whereas CS/Ag$^+$ ion films with approximately 2 wt.% of silver content denoted a maximum in bactericide effectiveness, thus suggesting that low concentration of AgNP's or Ag$^+$ is sufficient for cell death. These values correlated well with the percolation thresholds obtained from electrical measurements (0.85 ± 0.31 wt.% of silver for CS/AgNP's films and 1.51 ± 0.21 wt.% for CS/Ag$^+$ ion films). Above this critical concentration the antibacterial activity saturates or decreases against both Gram-positive *S. aureus* and Gram-negative *E. coli*. Both type of films showed the maximum bactericidal effectiveness close to percolation thresholds. The percolation effect helps to explain the observed maximum bactericide activity of the CS/AgNP's composites, i.e. once the system percolate, a physical path is formed through which the current can flow thus decreasing the effective surface area of nanoparticles [64]. Additionally, at higher silver concentrations, clusters start to appear which further decrease the surface area of nanoparticles (see Figs. 2 and 3). A similar observation has been reported in our previous studies with composites of chitosan with commercial AgNP [64].

The published literature is controversial about antibacterial properties of silver nanoparticles and silver ions. The various observed and hypothesized interactions between AgNP, Ag$^+$ ions and bacteria cells have been discussed in a large number of publication [28,66,67]. Some investigation showed that AgNP affects more the bacteria than silver ions, and the dominating factor is the direct contact of bacteria with nanoparticles [38]. In another publication it is proposed that nanosilver alone has minimal toxicity and it serves mostly as a source of Ag$^+$ ions [28,68]. Other publication supported the hypothesis of similar biological response of AgNP and Ag$^+$ ions [27].

Sotiriou and Pratsinis [28] proposed that the mechanism of antibacterial activity depends on nanoparticle size: the smaller AgNP releases higher concentration of Ag$^+$ ions. Thus, the antibacterial activity is dominated by the release of Ag$^+$ ions rather than by the AgNP itself. However it has been demonstrated that silver dendritic nanostructures possess a better antibacterial activity than that of silver nanosphere due to the large surface area, which provides an effective contact with the microorganisms (possibly to release silver ions that can penetrate inside the bacterial cell). Besides, such Ag dendritic nanostructures with numerous tips and inflection points could enhance bactericidal activity as well [69,70].

Herein, the results showed that CS/AgNP films (AgNP size less than 10 nm) have higher antibacterial activity than CS/Ag$^+$ ion films. In other investigation, CS/Ag^0 membrane surface (metallic Ag produced by chemical reduction with ascorbic acid) exhibited better antibacterial performance than the CS/Ag$^+$ after 4 days of inoculation, in agreement with our work [53]. In Ag/SiO_2 composite, the antibacterial activity of nanosilver was dominated by Ag$^+$ ions when Ag nanoparticles were less than about 10 nm in average diameter [28]. Further, the results here presented do not contradict the fact that silver dendritic nanostructures have showed a better antibacterial activity than that of silver nanosphere [69,70]. Those dendritic structures consisted of silver nanoparticles, but the dendritic structures in this work consist of silver acetate complex with chitosan as a source of Ag$^+$ ions.

The exact mechanism in which silver nanoparticles operate to cause antimicrobial effect is not clearly known. One possible antibacterial mechanism involves the interaction of silver with the bacteria cell wall and subsequent penetration; thereby causing structural changes in the cell membrane. Another plausible scenario is that, because the DNA of the bacteria has sulfur and phosphorus as its major components, the nanoparticles can act on these soft bases destroying the DNA and causing cell death [66,67].

CS/AgNP antibacterial properties can be explained as a synergistic effect of chitosan (which causes a decrease of about two orders of magnitude of CFU/cm^2 of *S. aureus* after 48 h of cell culture) and silver nanoparticles.

Chitosan stabilize the AgNP and prevent silver nanoparticle agglomeration below a critical concentration. It also confers a positive charge to nanoparticles surface, enhancing their binding to the negative charges present at the cell surface [42]. Moreover, the antibacterial activity increases with the concentration of AgNP and Ag$^+$ ions. We verified that close to percolation threshold, the antibacterial activity attained a maximum, suggesting higher effective surface area of silver nanoparticles because chitosan prevents AgNP aggregation. This in turns results in an effective interaction against bacteria cell wall. Above percolation concentration the presence of agglomerates dramatically lowers the effective surface area of both AgNP and Ag$^+$ ions and thus the antibacterial efficacy greatly decreased.

4. Conclusion

In summary, stable CS/AgNP and CS/Ag$^+$ ion bionanocomposite were successfully synthesized by a greener *in situ* chemical approach. The resulting bionanocomposites exhibit antibacterial activity against Gram-positive *S. aureus* and Gram-negative *E. coli* bacteria; the maximum bactericidal effect was reached by films containing 1 wt.%

of silver nanoparticles and about of 2 wt.% of silver ions. CS/AgNP composite showed a higher synergetic antibacterial action (ca. two orders of magnitude) compared to the CS/Ag^+ ion composites with the same concentration of silver. Thus, collective action of AgNP and Ag^+ ions (the latter present in the surface of AgNPs) facilitated the enhancement of synergetic antibacterial activity below critical concentration. On the other hand, chitosan helps stabilize the AgNP and prevents AgNP agglomeration below a critical concentration. Chitosan also confers a positive charge to nanoparticles surface, enhancing their binding to the negative charges present in the cell wall. The electrical and antibacterial properties of CS/AgNP and CS/Ag^+ ions bionanocomposite depend on the concentration. Above percolation threshold concentration, agglomeration of AgNP and Ag^+ ions is responsible for a decreasing in the effective surface area of AgNP and consequently the antibacterial activity. Finally, the *in situ* greener synthesis of CS/AgNP and CS/Ag^+ ions nanocomposites showed the sufficient antibacterial property against Gram-positive and Gram-negative bacteria such that they can be used for food and biomedicine industries.

Acknowledgements

This work was partially supported by CONACYT of Mexico. The authors are grateful to J.A. Muñoz-Salas for technical assistance in electrical measurements, R.A. Mauricio Sánchez for assistance in FTIR measurements and Ma. Lourdes Palma Tirado (Campus UNAM Juriquilla, Qro) for TEM Measurements.

References

[1] Salata OV. J Nanobiotechnol 2004;2:1–6.
[2] Panáček A, Kvítek L, Prucek R, Kolář M, Večeřová R, Pizúrová, et al. J Phys Chem 2006;110:16248–53.
[3] Kalele SA, Ashtaputre SS, Hebalkar NY, Gosavi SW, Deobagkar DN, Deobagkar DD, et al. Chem Phys Lett 2005;404:136–41.
[4] Yoshida K, Tanagawa M, Atsuta M. J Biomed Mater Res 1999;47:516–22.
[5] Hong KH, Park JL, Youk JH, Kang TJ. J Polym Sci: Part B: Polym Phys 2006;44:2468–74.
[6] Kelly FM, Johnston JH. ACS Appl Mater Interfaces 2011;3:1083–92.
[7] Sanpui P, Murugadoss A, Prasad PVD, Ghosh SS, Chattopadhyay A. Int J Food Microbiol 2008;124:142–6.
[8] Thomas V, Yallapu MM, Sreedhar B, Bajpai S. J Biomater Sci 2009;20:2129–44.
[9] Rai M, Yadav A, Gade A. Biotechnol Adv 2009;27:76–83.
[10] An J, Luo Q, Yuan X, Wang D, Li X. J Appl Polym Sci 2011;120:3180–9.
[11] Tran HV, Tran LD, Ba CT, Vu HD, Nguyen TN, Pham DG, et al. Colloid Surf A: Physicochem Eng Aspects 2010;360:32–40.
[12] Bozanic DK, Trandafilovic LV, Luyt AS, Djokovic V. React Funct Polym 2010;70:869–73.
[13] Sun RW, Chen R, Chung NP, Ho CM, Lin CL, Chen CM. Chem Comun 2005;40:5059–61.
[14] Toshima N, Yonezawa T. New J Chem 1998;22:1179–201.
[15] Kvitek L, Panacek A, Soupukova J, Kolar M, Vecerova R, Prucek R, et al. J Phys Chem C 2008;112:5825–34.
[16] Dallas P, Zboril R, Bourlinos B, Jancik D, Niarchos D, Panacek A, et al. Macromol Mater Eng 2010;295:108–14.
[17] Lu S, Gao W, Gu HY. Burns 2008;34:623–8.
[18] Mi FL, Wu YB, Shyu SS, Chao AC, Lai JY, Su CC. J Membr Sci 2003;212:237–54.
[19] Vimala K, Mohan YM, Sivudu KS, Varaprasad K, Ravindra S, Reddy NN, et al. Colloid Surf B: Biointer 2010;76:248–58.
[20] Zanse MVD, Vandebriel RJ, Doren EV, Kramer E, Rivera ZH, Serrano-Rojero CS, et al. ACS Nano 2012;6:7427–42.
[21] Liu J, Sonshine DA, Shervani S, Hurt RH. ACS Nano 2010;4:6903–13.
[22] Liu J, Hurt RH. Environ Sci Technol 2010;44:2169–75.
[23] Triebel C, Vasylyev S, Damm C, Stara H, Ozpinar C, Hausmann S, et al. J Mater Chem 2011;21:4377.
[24] Tamboli MS, Kulkarni MV, Patil RH, Gade WN, Navale Eval SC, Kale BB. Colloid Surf B: Biointer 2012;92:35–41.
[25] Xiu ZM, Ma J, Alvarez PJJ. Environ Sci Technol 2011;45:9003–8.
[26] Jung WK, Koo HC, Kim KW, Shin S, Kim SH, Park YH. Appl Environ Microbiol 2008;74:2171–8.
[27] Greulich C, Braun D, Peetsch A, Diendorf J, Siebers B, Epple M, et al. RSC Adv 2012;2:6981–7.
[28] Sotiriou GA, Pratsinis SE. Environ Sci Technol 2010;44:5649–54.
[29] Sharma VK, Yngard RA, Lin Y. Adv Coll Interf Sci 2009;145:83–96.
[30] Morones JR, Elechiguerra JL, Camacho A, Holt K, Kouri JB, Tapia RJ. Nanotechnology 2005;16:2346–53.
[31] Jia XP, Ma XY, Wei DW, Dong J, Qiam WP. Colloid Surf A: Physicochem Eng Aspects 2008;330:234–40.
[32] Dos Santos DS, Goulet PJG, Pieczonka NPW, Oliveira ON, Aroca RF. Langmuir 2004;20:10273–7.
[33] Wu WT, Pang W, Xu G, Shi L, Zhu Q, Wang Y, et al. Nanotechnology 2005;16:2048–51.
[34] Gaddy GA, McLain JL, Steigerwalt ES, Broughton R, Slaten BL, Mills G. J Cluster Sci 2001;12:457–71.
[35] Swatek AL, Dong Z, Shaw J, Rafiq Islam M. J Exp Nanosci 2010;5:10–6.
[36] Guibal E. Sep Purif Technol 2004;38:43–74.
[37] Varma AJ, Deshpande SV, Kennedy JF. Carbohydr Polym 2004;55:77–93.
[38] Jiang XC, Chen WM, Chen CY, Xiong SX, Yu AB. Nanoscale Res Lett 2011;6:2–9.
[39] Reicha FM, Sarhan A, Abdel-Hamid MI, El-Sherbiny IM. Carbohydr Polym 2012;89:236–44.
[40] Hu Y, Wu Y, Cai J, Ma Y, Wang B, Xia K, et al. Int J Mol Sci 2007;8:1–12.
[41] Jin L, Bai RB. Langmuir 2002;18:9765–70.
[42] Potara M, Jakab E, Darmert A, Popescu O, Canpean V, Astilean S. Nanotechnology 2011;22:135101.
[43] Lagaron JM, Fernández-Saiz P, Ocio MJ. J Agric Food Chem 2007;55:2254–562.
[44] Wei D, Sun W, Qian W, Ye Y, Ma X. Carbohydr Polym 2009;344:2375–82.
[45] Modrzejewska Z, Dorabialska M, Zarzycki R, Wojtasz-Pajcek A. Progr Chem Appl Chitin 2009;XIV.
[46] Mikhaylichenko K, Riehn C, Valachovic L, Sanov A, Wittig C. J Chem Phys 1996;16:6807–17.
[47] Bogle KA, Dhole SD, Bhoraskar VN. Nanotechnology 2006;17:3204.
[48] Fan LH, Du YM, Zhang BZ, Yang JH, Zhou JP, Kennedy JF. Carbohydr Polym 2006;65:447.
[49] Kunz C, Koch EE, Wertheim GK, Hochst H, Ley L, Campagna M, Cardona M, editors. Photoemission in solids II: case studies. Topics in applied physics, vol. 27. Berlin Heidelberg, New-York: Springer-Verlag; 1979.
[50] Prietoa P, Nistora V, Nounehb K, Oyamac M, Abd-Lefdild M, Diaz R. Appl Surf Sci 2012;258:8807–13.
[51] Morales J, Sánchez L, Martín F, Ramos-Barrado JR, Sánchez M. J Electrochem Soc 2004;151:151–7.
[52] Selvakannan PR, Swami A, Srisathiyanarayanan D, Shirude PS, Pasricha R, Mandale AB, et al. Langmuir 2004;20:7825–36.
[53] Zhu X, Bai R, Wee KH, Liu C, Tang SL. J Membr Sci 2010;363:278–86.
[54] Kaspar TC, Droubay T, Chambers SA, Bagus PS. J Phys Chem C 2010;114:21562–71.
[55] González-Campos JB, Prokhorov E, Luna-Bárcenas G, Sanchez IC, Lara-Romero J, Mendoza-Duarte ME. J Polym Sci: Part B: Polym Phys 2010;48:739–48.
[56] Bakeeva IV, Kolesnikova YA, Kataeva NA, Zaustinskaya KS, Gubin SP, Zubov VP. Russ Chem Bull 2008;57:337.
[57] Prokhorov E, Luna-Barcenas JG, Gonzalez-campos JB, Sanchez IC. Mol Cryst Liq Cryst 2011;536:256–64.
[58] Kirkpatrick S. Mod Phys 1973;45:574–88.
[59] Stauffer D. Introduction to Percolation Theory. 2nd ed. Taylor & Francis: London, Philadelphia; 1992.
[60] Jurewicz I, Worajittiphon P, King AAK, Sellin PJ, Keddie JL, Dalton AB. J Phys Chem B 2011;115:6395–400.
[61] Rabea EI, Badawy MET, Stevens CV, Smagghe G, Steurbaut W. Biomacromolecules 2003;4(6):1457.
[62] Sansone F, Picerno P, Mencherini T, Porta A, Lauro MR, Russo P, et al. J Food Eng 2014;120:260–7.
[63] Kong M, Chen XG, Xing K, Park HJ. Int J Food Microbiol 2010; 144:51–63.

[64] González-Campos JB, Mota-Morales JD, Kumar S, Zárate-Triviño D, Hernández-Iturriaga M, Prokhorov E, et al. Colloid Surf B: Biointer 2013;111:741–6.
[65] Kim JS, Kuk E, Yu KN, Kim JH, Park SJ, Lee HJ, et al. Nanomed: Nanotechnol BioMed 2007;3:95.
[66] Ahamed M, AlSalhi MS, Siddiqui MKJ. Clin Chim Acta 2010;411:1841–8.
[67] Prabhu S, Poulose EK. Intern Nano Lett 2012;2:32.
[68] Carlson C, Hussain SM, Schrand AM, Braydich-stolle LK, Hess KL, Jones RL, et al. J Phys Chem 2008;112:13608–19.
[69] Li HB, Liu P, Liang Y, Xiao J, Yang GW. Nanoscale 2012;4:5082–91.
[70] Xiong R, Lu C, Zhang W, Zhou Z, Zhang X. Carbohydr Polym 2013;95:214–9.